# Dynamical properties of z ∼ 4.5 dusty star-forming galaxies and their connection with local early type galaxies

Francesca Rizzo[1,2,3,★] Simona Vegetti[1], Filippo Fraternali[4], Hannah Stacey[1], Devon Powe
[1]Max-Planck Institute for Astrophysics, Karl-Schwarzschild Str. 1, D-85748, Garching, Germany
[2]Cosmic Dawn Center (DAWN), Jagtvej 128, DK2200, Copenhagen N, Denmark
[3]Niels Bohr Institute, University of Copenhagen, Lyngbyvej 2, DK-2100 Copenhagen Ø, Denmark
[4]University of Groningen, Kapteyn Astronomical Institute, Postbus 800, 9700 AV Groningen, The Netherlands



Accepted XXX. Received YYY; in original form ZZZ

**ABSTRACT**

There is a large consensus that gas in high-$z$ galaxies is highly turbulent, because of a combination of stellar feedback processes and gravitational instabilities driven by mergers and gas accretion. In this paper, we present the analysis of a sample of five Dusty Star Forming Galaxies (DSFGs) at $4 \lesssim z \lesssim 5$. Taking advantage of the magnifying power of strong gravitational lensing, we quantified their kinematic and dynamical properties from ALMA observations of their [CII] emission line. We combined the dynamical measurements obtained for these galaxies with those obtained from previous studies to build the largest sample of $z \sim 4.5$ galaxies with high-quality data and sub-kpc spatial resolutions, so far. We found that all galaxies in the sample are dynamically cold, with rotation-to-random motion ratios, $V/\sigma$, between 7 to 15. The relation between their velocity dispersions and their star-formation rates indicates that stellar feedback is sufficient to sustain the turbulence within these galaxies and no further mechanisms are needed. In addition, we performed a rotation curve decomposition to infer the relative contribution of the baryonic (gas, stars) and dark matter components to the total gravitational potentials. This analysis allowed us to compare the structural properties of the studied DSFGs with those of their descendants, the local early type galaxies. In particular, we found that five out of six galaxies of the sample show the dynamical signature of a bulge, indicating that the spheroidal component is already in place at $z \sim 4.5$.

**Key words:** galaxies: evolution – galaxies: high-redshift – galaxies: ISM – galaxies: kinematics and dynamics – submillimetre: galaxies – gravitational lensing: strong

## 1 INTRODUCTION

Within the framework of current galaxy formation and evolutionary models, galaxies grow by acquiring material through gas accretion lar mass growth, as well as in determining the resulting kinematic and chemical properties of galaxies, is still a matter of debate (e.g. Oesch et al. 2010; Satyapal et al. 2014; Eliche-Moral et al. 2018).

# В чем проблема?

Проблема формирования галактик: что регулирует рост массы?.

- Feedback (AGN, SF), merging, gas outflow.

Наблюдения на больших z: проблема угл.разрешения.

Выход**: strongly lensed galaxies.**

- Предыдущая работа: Rizzo et al, 2020:  A lensed dusty star-forming galaxy (DSFG), SPT0418, at $z$ = 4.2. In particular, they found that SPT0418-47 has dynamical properties similar to those of local spiral galaxies: it is rotationally supported and has a low level of turbulence, that is, it is dynamically cold.
- Fraternali et al. (2020) obtained a similar result for two non-lensed DSFGs at $z$  4.5.
- In this paper, we present the analysis of a sample of five Dusty Star Forming Galaxies (DSFGs) at $4 < z < 5$.
- The five lensing system of our selected sample were identified in the South Pole Telescope (SPT) survey

**НАБЛЮДЕНИЯ:** ALMA, 158-$\mu$m [CII] emission line. Resolution < 0.3’’.

- 158-$\mu$m [CII] emission line, ударное возбуждение основного уровня.

More than 60 percent of the [CII] emission originates in the photodissociation regions, the external layers of molecular clouds heated by the far ultraviolet photons emitted from OB stars.

A wide range of physical conditions makes [CII] an excellent tracer of the kinematics of high-$z$ star-forming galaxies over large areas of their discs.

- For the sample studied in this paper, the minimum spatial resolutions range from  20 to 130 pc and the median spatial resolutions range from  170 to 300 pc.

# Кинематическая модель

$$R\left(\frac{\partial \Phi}{\partial R}\right)_{z=0} = V_c^2 = V_{rot}^2 + V_A^2, \quad V_c = \sqrt{V_{star}^2 + V_{gas}^2 + V_{DM}^2},$$

For all but one of the sources in the sample, we adopted a multiparameter function for their rotation curve

$$V_{rot}(R) = V_t \frac{\left(1 + \frac{R_t}{R}\right)^{\beta}}{\left[1 + \left(\frac{R_t}{R}\right)^{\xi}\right]^{1/\xi}}.$$

- In contrast, we found that for SPT2132-58 a simpler arctg function,

$$V_{rot}(R) = \frac{2}{\pi} V_t \arctan\left(\frac{R}{R_t}\right),$$

We assume the ve urve to have an exponential profile $\sigma(R) = \sigma_0 e^{-\frac{R}{R_\sigma}}$.

Наблюдаемая картина

Восстановленная картина

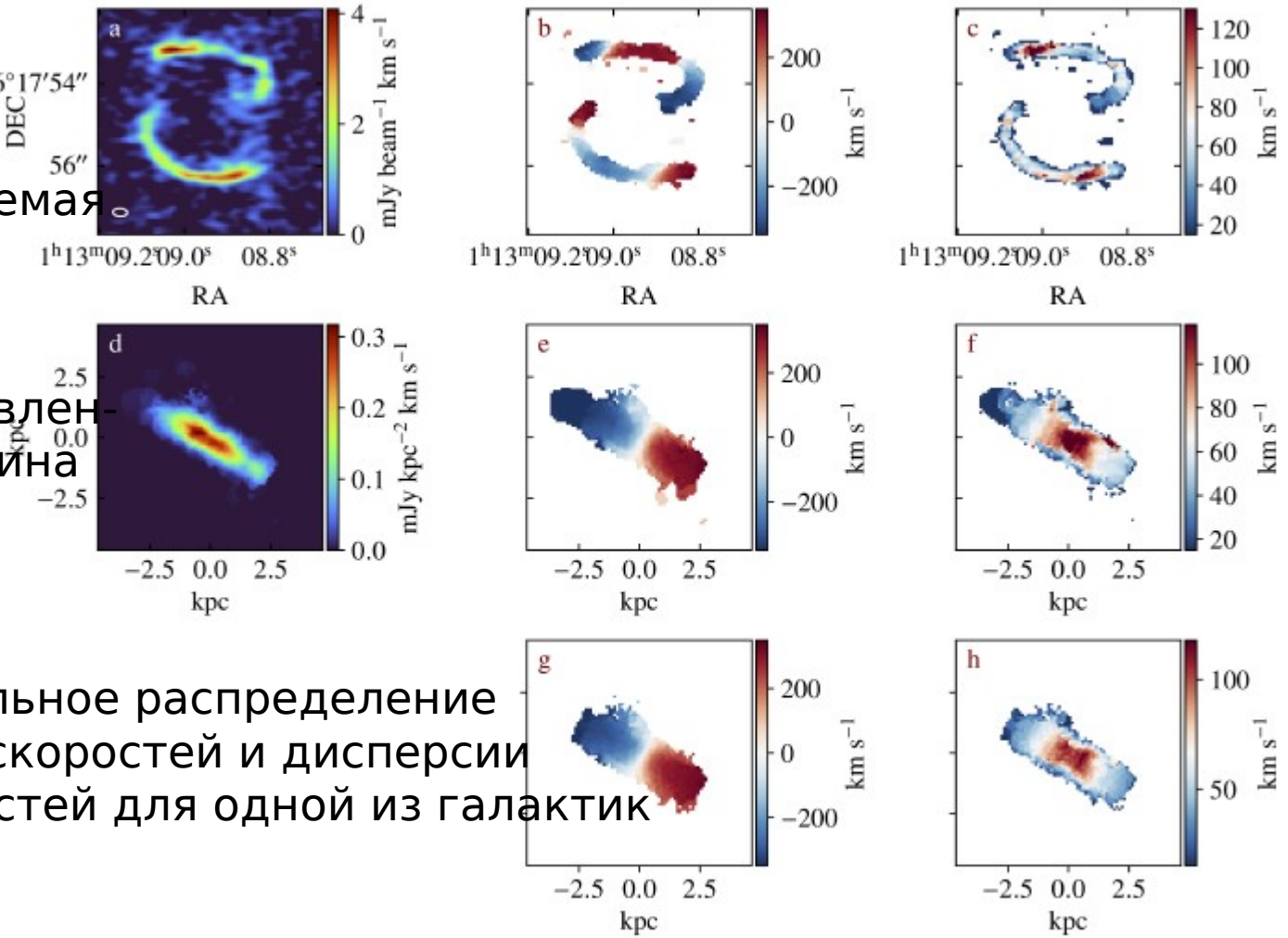


Модельное распределение поля скоростей и дисперсии скоростей для одной из галактик

**Figure 1.** Moment maps for SPT0113-46. Panels a, b and c: the observed [CII] zeroth-, first- and second-moment maps. The beam size, shown as a white ellipse on the lower left corner of panel a, is $0.35 \times 0.19$ arcsec$^2$ at a position angle of 87.0°. Panels d, e and f: zeroth-, first- and second-moment maps of the reconstructed source. Panels g and h: first- and second-moment maps of the kinematic model. These maps are intended only for visualisation as the full analysis is performed on the data cube.

SFR: obtained from spectral energy distribution (SED) fitting of far-infrared and sub-millimeter observations, covering the range 250 to 3000 $\mu$m (Kroupa IMF).

**Table 6.** SFR and [CII] luminosities of the sources. Column two: the observed infrared luminosity from Aravena et al. (2016). Column three: the magnification factor of the continuum in the infrared bands. Column four: star-formation rate derived for a Kroupa IMF. Column five: intrinsic [CII] luminosities.

| Name | $L_{IR,obs}$ $10^{13}$ $L_\odot$ | $\mu$ | SFR $10^2 M_\odot$ yr$^{-1}$ | $L_{[CII]}$ $10^9$ $L_\odot$ |
|---|---|---|---|---|
| SPT0113-46 | 3.0±0.5 | 36.5±4.3 | 1.2±0.3 | 2.3±0.1 |
| SPT0345-47 | 13.0±2.4 | 14.5±1.2 | 13.3±2.6 | 2.3±0.2 |
| SPT0441-46 | 4.8±0.9 | 10.8±0.5 | 6.6±1.3 | 1.8±0.1 |
| SPT2146-56 | 3.6±0.8 | 7.8±0.2 | 6.8±1.5 | 2.6±0.2 |
| SPT2132-58 | 4.2±0.7 | 6.3±0.4 | 9.8±1.7 | 3.7±0.7 |

**The rotation curves of the galaxies analysed here have shapes similar to those of local spirals: they flatten at large radii and show a variety of behaviours in the inner regions, from slow to steeply rising**

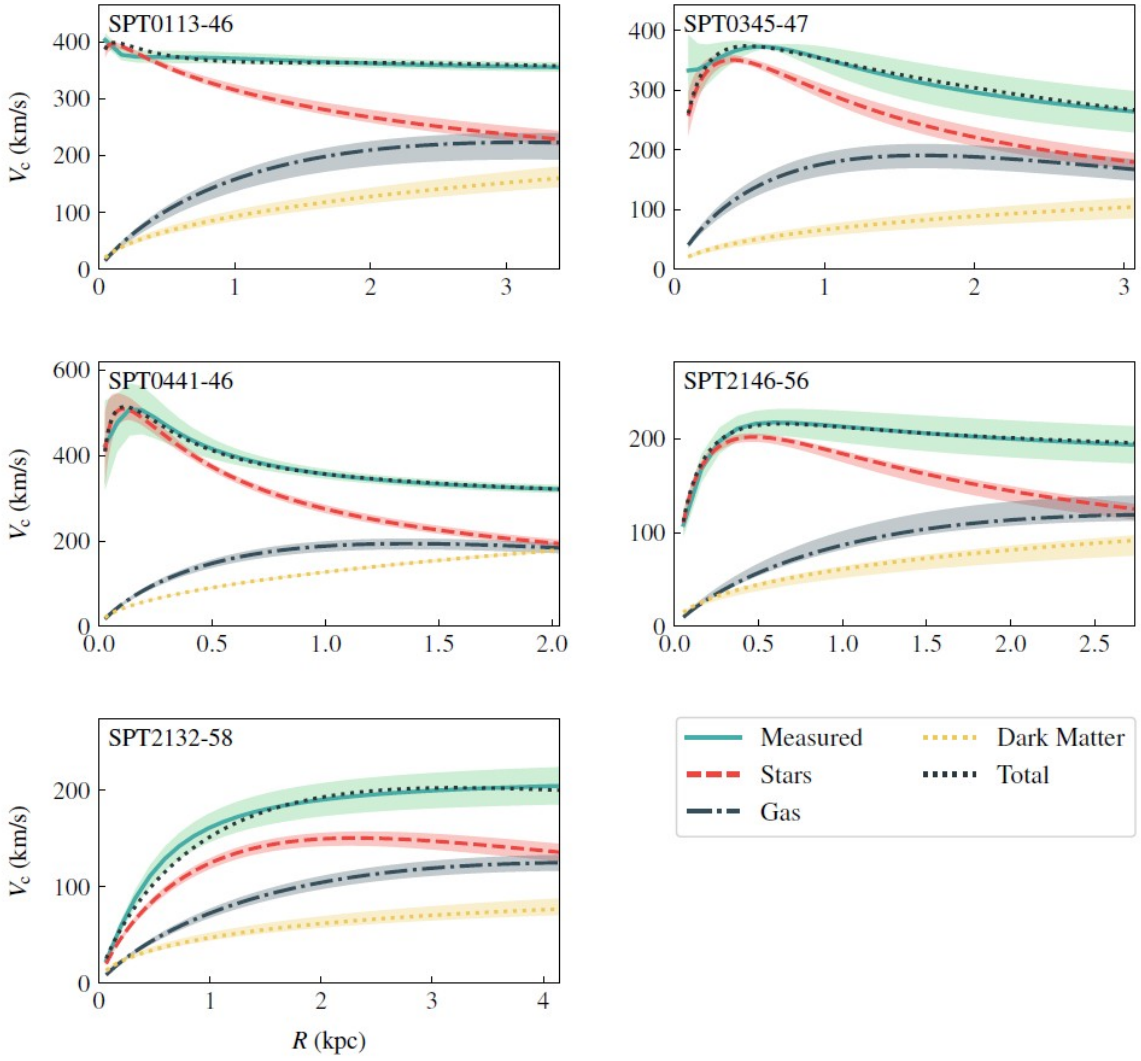


**Figure 4.** Rotation curve decomposition. The green solid lines show the circular velocity profiles. The black dotted lines show the best dynamical models, and the contribution from the different mass components as indicated by the legend and listed in Tables 4 and 5.

# Результирующие оценки

rom left to right the gas mass, the fraction of total baryonic mass in gas, ne total baryonic mass, the baryonic effective radius, the gas depletion time nd the disc-scale height.

| Name | $M_{gas}$ $10^{10}$ $M_\odot$ | $f_{gas}$ | $M_{bar}$ $10^{10}$ $M_\odot$ | $R_{bar}$ kpc | $t_{dep}$ Myr | $h$ pc |
|---|---|---|---|---|---|---|
| SPT0113-46 | $4.3^{+1.0}_{-0.9}$ | $0.39^{+0.11}_{-0.09}$ | $10.9^{+1.2}_{-1.1}$ | $2.2^{+0.4}_{-0.2}$ | 357± 73 | $100^{+86}_{-36}$ |
| SPT0345-47 | $1.7^{+0.4}_{-0.4}$ | $0.42^{+0.08}_{-0.09}$ | $4.0^{+0.3}_{-0.3}$ | $0.64^{+0.07}_{-0.05}$ | 12± 2 | $351^{+88}_{-88}$ |
| SPT0441-46 | $1.4^{+0.2}_{-0.2}$ | $0.45^{+0.05}_{-0.06}$ | $3.2^{+0.2}_{-0.2}$ | $0.35^{+0.06}_{-0.05}$ | 22±4 | $225^{+105}_{-84}$ |
| SPT2146-56 | $1.2^{+0.3}_{-0.2}$ | $0.54^{+0.07}_{-0.08}$ | $2.2^{+0.2}_{-0.2}$ | $1.3^{+0.2}_{-0.2}$ | 17±4 | $324^{+99}_{-73}$ |
| SPT2132-58 | $1.9^{+0.3}_{-0.3}$ | $0.50^{+0.07}_{-0.07}$ | $3.9^{+0.4}_{-0.3}$ | $2.47^{+0.13}_{-0.12}$ | 20±4 | $368^{+90}_{-74}$ |

$$h(R) = \frac{\sigma(R)}{\sqrt{4\pi G[\rho(R) + \rho_{rot}(R)]}}$$

**Table 8.** Global kinematic parameters of the sources. Column two: the maximum rotation velocity. Column three: the median velocity dispersion. Column four: the ratio between $V_{max}$ and $\sigma_m$. Column five: the rotation velocity in the flat part of the rotation curve. Column six: the velocity dispersion in the external regions ($R \gtrsim R_e$). Column seven: the ratio between $V_{flat}$ and $\sigma_{ext}$.

| Name | $V_{max}$ | $\sigma_m$ | $V_{max}/\sigma_m$ | $V_{flat}$ | $\sigma_{ext}$ | $V_{flat}/\sigma_{ext}$ |
|---|---|---|---|---|---|---|
| SPT0113-46 | 382±9 | 41±22 | 9.2±4.8 | 358±3 | 27±1 | 13.2±0.6 |
| SPT0345-47 | 373±5 | 66±15 | 5.6±1.2 | 280±25 | 40±7 | 6.9±1.4 |
| SPT0441-46 | 489±67 | 31±21 | 15.8±10.8 | 342±4 | 23±4 | 14.9±2.6 |
| SPT2146-56 | 217±13 | 31±11 | 7.0±2.6 | 194±7 | 20±2 | 9.8±1.2 |
| SPT2132-58 | 199±18 | 27±6 | 7.2±1.7 | 196±14 | 16±3 | 12±2 |

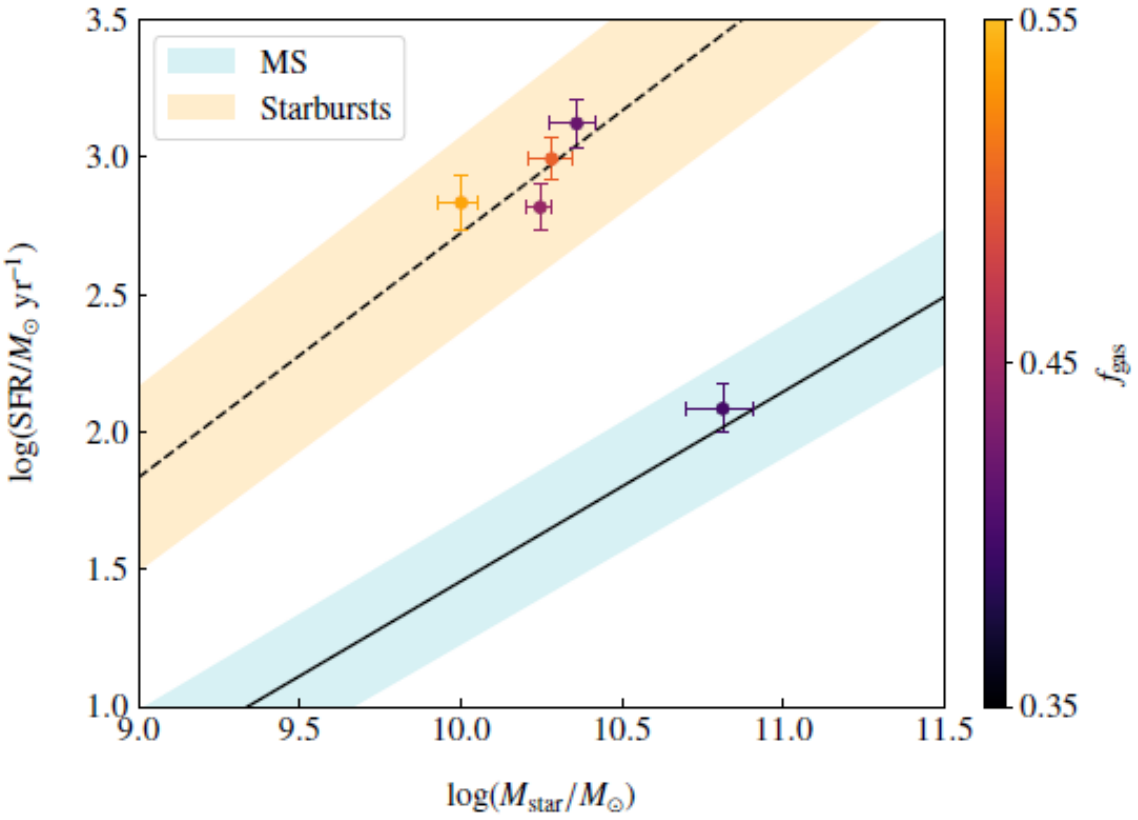


**Figure 5.** Location on the SFR - $M_{\rm star}$ of the source galaxies in our sample (circles), with markers colour-coded according to their gas fraction. The solid black line and the blue area show the best-fit and the 1-$\sigma$ scatter for main-sequence galaxies at $z \sim 4$ - 5 from Caputi et al. (2017), respectively. The dotted black line and the orange area show the starburst sequence.

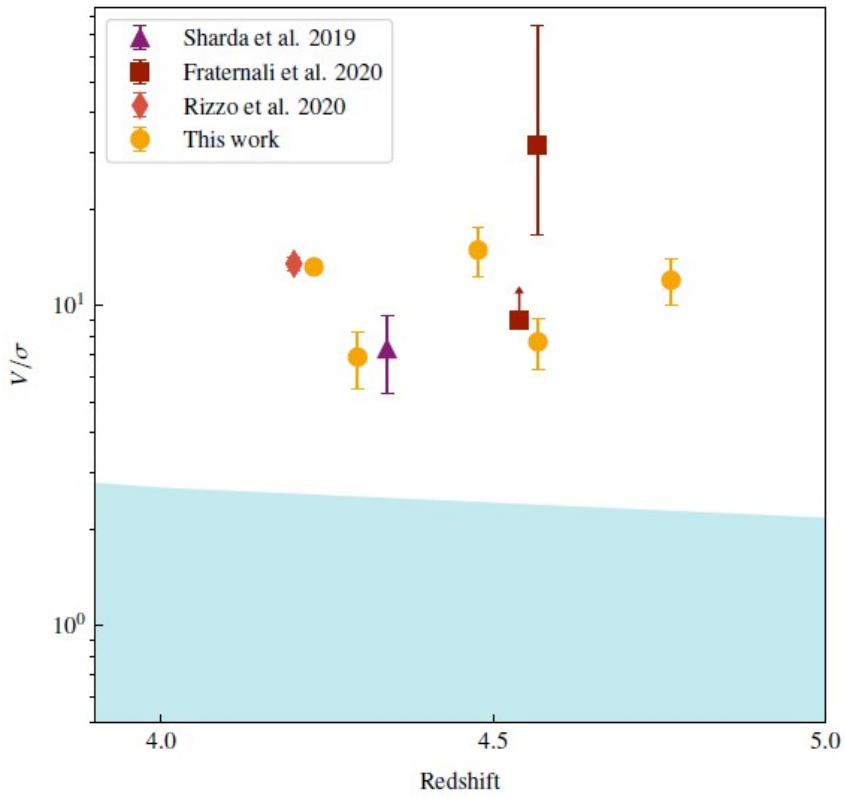


**Figure 6.** $V/\sigma$ versus redshift. The $V/\sigma$ for our sample (yellow circles), defined as $V_{\rm flat}/\sigma_{\rm ext}$ and for the galaxies from literature (Table 7), as indicated in the legend. Note that the redshift of SPT0418-47 (orange diamond) is shifted by -0.02 for a better visualisation of all the points. The light-blue area shows the region covered by theoretical studies (Pillepich et al. 2019; Dekel & Burkert 2014; Zolotov et al. 2015; Hayward & Hopkins 2017).

e ratios of $V/\sigma$ are similar to those measured for spiral galaxies in the local Univer
lli et al. 2016; Bacchini et al. 2019).

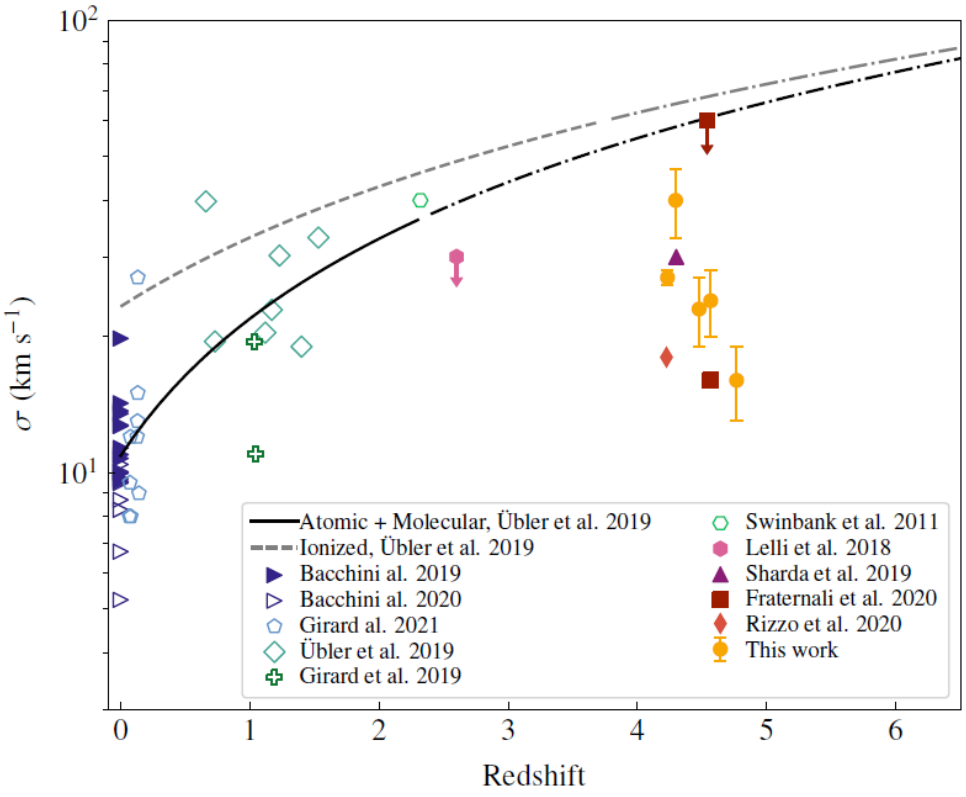


**Figure 9.** Location on the velocity dispersion versus redshift plane of the source galaxies in our sample. The values of $\sigma_{\rm ext}$ (column 6 in Table 8) are shown here. The blue filled right triangles are velocity dispersions from HI data (Bacchini et al. 2019). The empty markers are CO velocity dispersions (Bacchini et al. 2020; Girard et al. 2021; Übler et al. 2019, 2018; Girard et al. 2018; Swinbank et al. 2011) . The filled markers at $z \gtrsim 3$ are velocity dispersions from the [CI] (Lelli et al. 2018) or [CII] emission lines (Sharda et al. 2019; Fraternali et al. 2020; Rizzo et al. 2020). The black solid and gray dotted lines show the best-fit relations to velocity dispersions measured from warm ionized tracers (H$\alpha$, [OII], [OIII]) and atomic (HI)/molecular (CO) tracers (Übler et al. 2019). The dot-dashed lines show the corresponding extrapolations up to $z \approx 6$.

# Можно ли объяснить наблюдаемую дисперсию скоростей вспышками SN?

$$\sigma_{\rm SFR} = 58 \left(\frac{\epsilon_{\rm SN}}{0.1} \frac{\rm SFR}{300 M_\odot {\rm yr}^{-1}} \frac{h}{200{\rm pc}}\right)^{1/3} \left(\frac{M_{\rm gas}}{10^{10} M_\odot}\right)^{-1/3} {\rm kms}^{-1}, \quad (11)$$

where $\epsilon_{\rm SN}$ is the efficiency of transferring kinetic energy from supernova feedback to the ISM and $h$ is the disc scale height. Equation (11) is obtained by assuming a supernova rate of 0.01 $M_\odot^{-1}$, valid for a Kroupa IMF (Tamburro et al. 2009)

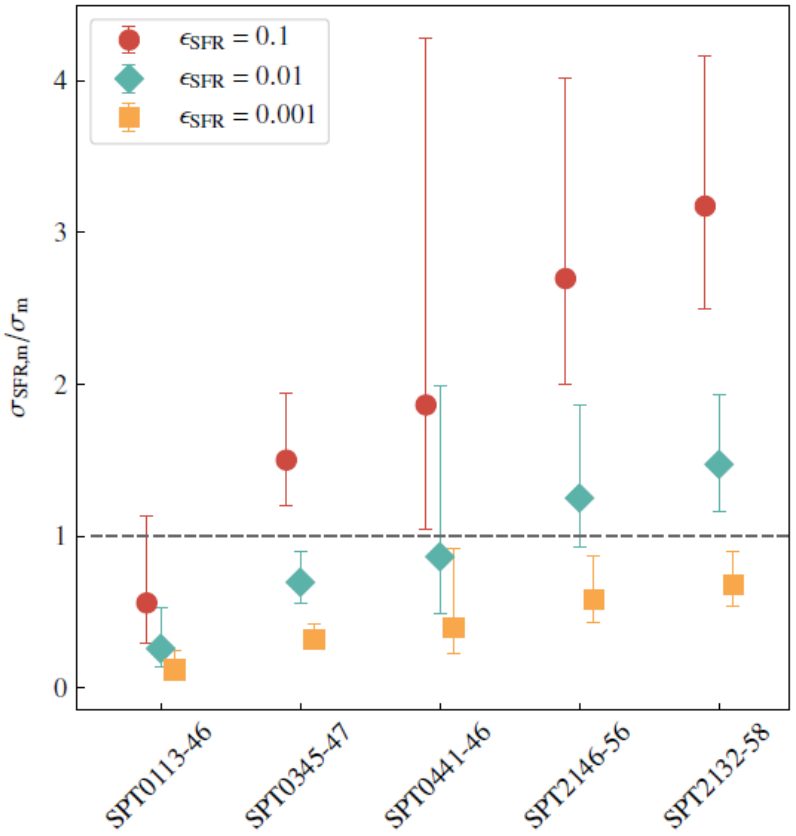


**Figure 8.** Ratio between the velocity dispersion expected from energy injection by the stellar feedback, equation (11), and the measured velocity dispersion $\sigma_{\rm m}$ (column three in Table 8). The three markers for each galaxy show the ratios obtained with three different values of $\epsilon_{\rm SN}$, as indicated in the legend.

# Conclusions

- The sample studied in this paper allowed us to confirm a previous finding (Rizzo et al. 2020): DSFGs have $V/\sigma$ in the range 7 to 15 and median velocity dispersion in the range between 30 and 60 km/s. To date, such dynamically cold galaxies with the measured values of SFR and gas fractions are not predicted by any model.
- The median values of the velocity dispersions in our sample is only a factor of 2 larger than the typical HI velocity dispersions. We found that stellar feedback mechanisms are able to sustain the level of observed turbulence with low efficiency.
- The rotation curves of the galaxies analysed here have shapes similar to those of local spirals
- From the dynamical fitting, we found that the galaxies in our sample have a stellar-mass between $1\ 10^{10} M$ and $7\ 10^{10} M$. Their gas fraction ranges between 0.4 and 0.6.
- We also found that the baryonic masses in our sample are all consistent with

those of local ETGs . This result allowed us to set constraints on the small amount of baryonic matter that can be accreted in the following 12 Gyr of the lifetime of these galaxies.